ACS APPLIED MATERIALS & INTERFACES

Research Article

www.acsami.org

Ratiometric Monitoring of Intracellular Drug Release by an Upconversion Drug Delivery Nanosystem

Kai Li, Qianqian Su, Wei Yuan, Bo Tian, Bin Shen, Yuhao Li, Wei Feng, and Fuyou Li*

Department of Chemistry and The Institutes of Biomedical Sciences of Shanghai Medical School, Fudan University, Shanghai 200433, P. R. China

Supporting Information

ABSTRACT: Nanoscale drug delivery systems have been widely investigated due to their well-recognized advantages including controlled delivery of chemotherapeutic agents, enhanced therapeutic effectiveness, and reduced adverse effects compared to conventional chemotherapy with small molecules. However, further progress in the use of nanoscale delivery systems in clinical applications has been hampered by pharmacokinetic studies in biological samples which were associated with significant experimental challenges. Here, we report a rational ratiometric approach to monitor drug release kinetics by quantitatively investigating luminescence resonance energy transfer (LRET) from upconversion nanoparticles to the antitumor drug doxorubicin (DOX). Specifically, DOX molecules within the shell of mesoporous silica-coated upconversion nanoparticles selectively quenched the green emission of upconversion nanoparticles, while the intensity of red emission was essentially unaltered. Consequently, when DOX was gradually released, a steady recovery of green emission was observed. The ability to monitor the intensity ratio of green-to-red luminescence enabled a rational design for real-time investigation of drug delivery release kinetics. Importantly, the internal standard effect of red emission made this ratiometric approach suitable for complex biological microenvironments.

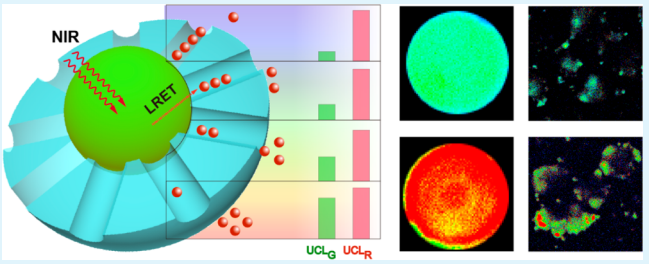

KEYWORDS: *upconverting luminescence, drug release, LRET, ratiometric, nanocarriers, monitoring, intracellular imaging*

INTRODUCTION

The enthusiasm for research on nanoscale drug delivery systems is driven by their potential biomedical applications in medical diagnostics and disease treatment with inherent advantages for reducing common chemotherapy-associated side effects.[1−4] Despite the remarkable progress made in the past decade, the pharmacokinetics of nanocarriers in biological environments are not well understood and consequently hamper their clinical applications.[5,6] The delivery of drugs at the required dose are critical for increasing therapeutic effectiveness.[4,7]

The extent of luminescence resonance energy transfer (LRET) heavily depends on the distance between the energy donor and acceptor, offering opportunities for sensing the nanocarrier−drug molecule distance in drug delivery systems. Importantly, LRET-based drug release monitoring systems provide unique advantages such as highly sensitive, real-time, and noninvasive systems. Currently, a number of LRET-based drug release monitoring approaches have been proposed.[8−18] However, most of these systems employ small-molecule organic dyes as the luminescent donor. The inevitable cellular photodamage, low-depth tissue penetration due to UV/visible light excitation as well as poor photostability and chemical stability limit their potential use in biomedical applications.

Alternatively, lanthanide-doped upconversion nanophosphors ($NaYF_4$:Yb,Er) have attracted considerable attention due to their inherent advantages of significant photostability, sharp emission bandwidths, large anti-Stokes shifts, long luminescence lifetime, and absence of autofluorescence under low energy near-infrared (NIR) excitation.[19−24] Notably, these nanoparticles are promising for bioapplications such as drug delivery,[25−32] bioimaging,[33−35] and biodetection.[36] Very recently, a few groups have demonstrated the rational strategy of upconversion nanophosphors-based drug delivery systems.[37−41] However, the vast majority of existing drug release monitoring approaches utilize emission intensity variability as the tracked signal which may be affected by an unknown local concentration of nanocarriers and uncontrolled microenvironment change in biological samples. As a result, the reported upconversion drug delivery systems are mainly focused on solution systems not living cells. Here, we present a rational design for ratiometric monitoring of drug release kinetics in living cells through upconversion-based LRET process, using mesoporous silica-coated $NaYF_4$:Yb,Er nanocomposites loaded with doxorubicin ($NaYF_4$:Yb,Er@$mSiO_2$-DOX). In this work, the excited energy from the higher-lying energy level (green upconversion luminescence, UCL_G) of the $NaYF_4$:Yb,Er nanoparticles was selectively transferred to the drug DOX,

Received: April 14, 2015
Accepted: May 15, 2015
Published: May 15, 2015

DOI: 10.1021/acsami.5b03204
ACS Appl. Mater. Interfaces 2015, 7, 12278−12286

Scheme 1. Schematic Illustration of LRET-Based Upconversion Nanocarriers for DOX Delivery (Left) and the Linear Relationship between the DOX Release Percentage and UCL_G/UCL_R Ratio (Right)[a]

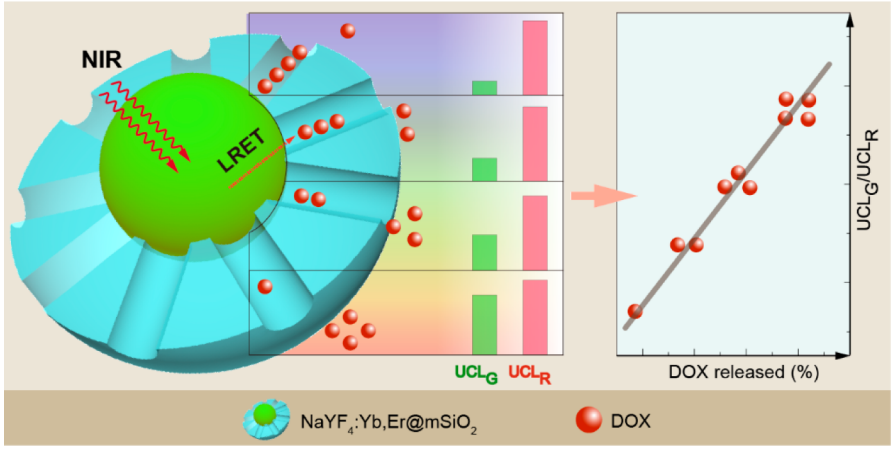

[a]UCL_G and UCL_R denote green and red upconversion luminescence, respectively.

through the LRET mechanism. In addition, the red upconversion emission (UCL_R) from the lower-lying energy level was essentially unchanged and used as an internal standard. We demonstrated how the ratio of the higher-lying UCL_G and lower-lying UCL_R intensity vary along with the process of drug release (Scheme 1). We found a linear relationship between the green-to-red emission intensity ratio (UCL_G/UCL_R) and the percentage of DOX released. More importantly, this ratiometric design employed red emission as the internal standard and thus may offer an accurate and reliable platform for localized drug delivery monitoring in living cells, avoiding the influence of the internal microenvironment and dosing errors.

RESULTS AND DISCUSSION

Synthesis of Oleic Acid (OA)-Capped $NaYF_4$:Yb,Er Nanocrystals. The oleic acid capped $NaYF_4$:Yb,Er nanoparticles (OA-$NaYF_4$:Yb,Er) were synthesized via a well-established solvothermal route.[25] The transmission electron microscopy (TEM) image shows a highly uniform spherical morphology of OA-$NaYF_4$:Yb,Er with an average diameter of 30 nm (Figure 1a). The OA-$NaYF_4$:Yb,Er demonstrated a hexagonal phase showed by the X-ray diffraction (XRD) study (Figure S1 in the Supporting Information, JCPDS card no. 16-0334), which is consistent with the observed lattice fringes of 0.51 nm associated with (100) planes in high-resolution HR-TEM image (Figure 1b).

Synthesis of $NaYF_4$:Yb,Er@$mSiO_2$. The mesoporous silica-coated $NaYF_4$:Yb,Er nanocomposite ($NaYF_4$:Yb,Er@$mSiO_2$) was successfully fabricated by coating mesoporous silica shell onto $NaYF_4$:Yb,Er nanoparticles according to a previously reported method.[42] As shown in Figure 1c and Figure S2 in the Supporting Information, the prepared $NaYF_4$:Yb,Er@$mSiO_2$ were confirmed with a uniform size by TEM and exhibited a mean hydrodynamic size of 80 nm by dynamic light scattering (DLS). Energy-dispersive X-ray (EDX) and elemental (Si, F) mapping analysis clearly confirmed that silica was successfully deposited onto the $NaYF_4$:Yb,Er nanoparticles surface (Figures S3 and S4 in the Supporting Information). It is should be noted that the thickness of mesoporous silica layer could be tuned by adding different amounts of tetraethylorthosilicate. For efficient energy transfer

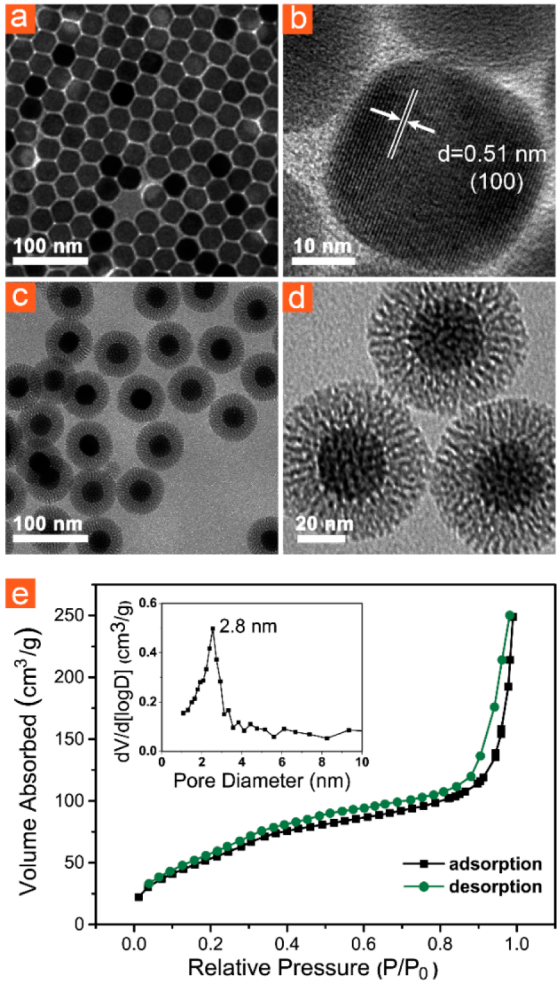

Figure 1. (a) TEM image and (b) HR-TEM image of the OA-$NaYF_4$:Yb,Er nanoparticles. (c) TEM image and (d) HR-TEM image of the $NaYF_4$:Yb,Er@$mSiO_2$ nanocomposites. (e) Nitrogen adsorption−desorption isotherm and pore diameter distribution (inset) of $NaYF_4$:Yb,Er@$mSiO_2$.

to proceed,[43] a thin mesoporous silica shell about 20 nm was used in our design as shown in Figure 1d. Nitrogen adsorption−desorption analysis was further employed to

DOI: 10.1021/acsami.5b03204
ACS Appl. Mater. Interfaces 2015, 7, 12278−12286

evaluate the pore volume and pore size in the mesoporous shell. The results showed that the silica shell had a pore volume of 0.43 cm^3/g of the total $NaYF_4$:Yb,Er@$mSiO_2$ mass with a pore size of 2.8 nm (Figure 1e). In addition, the surface area was estimated to be 344 m^2/g using the Barret-Joyner-Halenda (BJH) theory.

The upconversion emission spectra of the $NaYF_4$:Yb,Er nanoparticles and $NaYF_4$:Yb,Er@$mSiO_2$ nanocomposites under NIR irradiation at 980 nm were then measured and shown in Figure 2a. Both $NaYF_4$:Yb,Er and $NaYF_4$:Yb,Er@$mSiO_2$

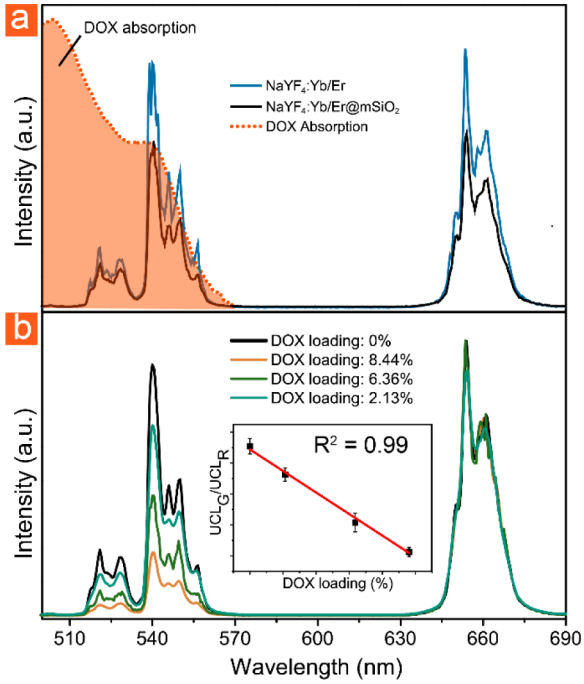

Figure 2. (a) Upconversion luminescence (UCL) spectra of the $NaYF_4$:Yb,Er nanoparticles in hexamethylene (1 mg/mL) and $NaYF_4$:Yb,Er@$mSiO_2$ in ethanol (1 mg/mL) and UV−vis absorption spectrum (solid orange) of DOX in water (50 μg/mL) containing 0.9% NaCl and 0.5% tween 80 (w/w). (b) The upconversion emission spectra of DOX-loaded $NaYF_4$:Yb,Er@$mSiO_2$ (1 mg/mL) with different amounts of DOX load efficiency. Inset: linear relationship between ratiometric UCL_G/UCL_R value and the loaded percentage of DOX.

nanomaterials exhibited characteristic green and red upconversion emissions from 510 to 570 nm and 630 to 690 nm, which can be attributed to $^2H_{11/2}$, $^4S_{3/2} \rightarrow {}^4I_{15/2}$, and $^4F_{9/2} \rightarrow {}^4I_{15/2}$ transitions of Er^{3+}, respectively. Furthermore, $NaYF_4$:Yb,Er@$mSiO_2$ nanocomposites exhibit high chemical stability and superior photostability compared with traditional luminescent nanocarriers.

Construction of LRET Pair and DOX Loading. For an efficient upconversion-based LRET system, the absorption wavelength of the energy acceptor should overlap with the upconversion emission of the upconversion nanophosphors. Herein, the drug DOX was chosen as the energy acceptor. The absorption curve of DOX was recorded by a UV−vis spectrophotometer. As shown in Figure 2a, an excellent spectral overlap between the absorption band of DOX and the emission from the higher-lying energy orbital of $NaYF_4$:Yb,Er nanoparticles was observed, providing an important prerequisite for LRET from upconversion nanoparticles to DOX.

Because of the high pore volume and high surface area of mesoporous silica shell, the $NaYF_4$:Yb,Er@$mSiO_2$ nanocomposites have the potential for drug adsorption. In a typical experiment, the drug DOX was encapsulated in the pores of the mesoporous silica shell by adding different amounts of DOX to the nanocomposite solution. As shown in Figures S5 and S6 in the Supporting Information, UV−vis absorbance curves and Fourier transform infrared spectroscopy (FTIR) spectra revealed the successful encapsulation of DOX into the mesopores of $NaYF_4$:Yb,Er@$mSiO_2$ nanocomposites.

Calculation of DOX Loading Efficiency by Upconversion LRET Process. The DOX loading efficiency was determined by measuring the variation of Abs. at 488 nm of DOX/DMSO solution before and after the loading process. Herein, by adjusting the amount of DOX added to the nanocomposites solution, the loading efficiency of DOX could be easily tuned. For example, when 4 mg/mL $NaYF_4$:Yb,Er@$mSiO_2$ nanocomposites and different concentrations (2 mg/mL, 4 mg/mL, 8 mg/mL) of DOX were mixed, the loading efficiency of DOX was determined to be 2.13%, 6.36%, and 8.44% (w/w), respectively, as shown in Figure 2b. Herein, DOX-loaded $NaYF_4$:Yb,Er@$mSiO_2$ was abbreviated as $NaYF_4$:Yb,Er@$mSiO_2$-DOX.

Because of the presence of the LRET process from green UCL to the absorption band of DOX, it is reasonable that $NaYF_4$:Yb,Er@$mSiO_2$-DOX with different DOX loading efficiency show the changed ratio of green/red upconversion intensities. Therefore, we studied the upconversion emission properties of our drug carrier with and without DOX loading under 980 nm laser irradiation. Expectedly, with the increase in DOX loading efficiency of $NaYF_4$:Yb,Er@$mSiO_2$-DOX, a steady decrease in green emission (510−560 nm) was observed, which was attributed to distinct energy transfer from green upconversion emission (UCL_G) to DOX (Figure 2b). In contrast, the intensity of red upconversion emission from 630 to 690 nm (UCL_R) remained constant, because there was no significant overlapping between red upconversion emission and DOX absorption band. Importantly, a linear relationship was found between the ratio of green upconversion emission to the red one (UCL_G/UCL_R) and the amount of drug loaded (Figure 2b, inset). As a result, such a standard curve was plotted as $UCL_G/UCL_R = 0.89-0.07w$. Herein, w stands for the DOX loading efficiency in $NaYF_4$:Yb,Er@$mSiO_2$. Taken together, we expect that construction of such a standard curve may provide an opportunity for the study of drug release kinetics and real-time sensing.

***In Vitro* Drug Release and Monitoring.** To verify whether this strategy can be used in drug release kinetics studies, we determined the release profile *in vitro* of DOX from the nanocarrier $NaYF_4$:Yb,Er@$mSiO_2$-DOX. In the cumulative release curve of DOX shown in Figure 3, a burst release of DOX within the first 5 h was observed from $NaYF_4$:Yb,Er@$mSiO_2$-DOX and then the release of DOX was stable. The percentage of DOX released was 50% and 88%, respectively, at time point of 3 and 14 h. After 14 h, a negligible amount of DOX was released.

Next, we compared a series of upconversion emission results at predetermined time points, as plotted in Figure 3 inset. Accompanying with the drug release process, the UCL_G intensity gradually recovered, while the UCL_R intensity remained unaltered. The recovered green emission was likely due to the reduced LRET efficiency caused by the increased

DOI: 10.1021/acsami.5b03204
ACS Appl. Mater. Interfaces 2015, 7, 12278−12286

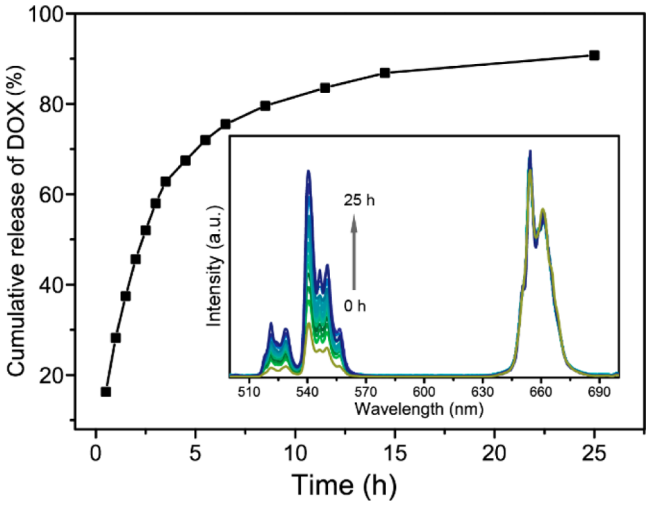

Figure 3. *In vitro* release of DOX from $NaYF_4$:Yb,Er@$mSiO_2$-DOX. Inset: change in upconversion emission spectra of $NaYF_4$:Yb,Er@$mSiO_2$-DOX at different time intervals (0−25 h) during DOX release process, under excitation at 980 nm.

distance between the upconversion nanoparticles donor and DOX acceptor along with the DOX release process.

To determine the capability of $NaYF_4$:Yb,Er@$mSiO_2$-DOX nanocomposite in studying the drug delivery kinetics *in vitro*, the relationship between DOX release and upconversion emission properties was analyzed. It is noteworthy that, with the prolongation of DOX release time, the same trend was observed in the UCL_G/UCL_R profile (Figure 4a). By analyzing available optical data, we obtained a linear relationship between UCL_G/UCL_R and the percentage of DOX released (Figure 4a inset). The potential of the ratiometric imaging method was examined by visualizing the drug release process in a 96-well plate using a small-animal upconversion emission imaging system.[24] We compared the UCL_G (500−600 nm), UCL_R (647−673 nm), and ratiometric (UCL_G/UCL_R) imaging as a function of DOX release time with 980 nm laser irradiation, as shown in Figure 4b. We noted that, in the $NaYF_4$:Yb,Er@$mSiO_2$-DOXgroup, the intensity of UCL_G/UCL_R imaging gradually increased and the ratiometric images exhibited good chromatic contrast during the course of DOX release. Whereas, in the control $NaYF_4$:Yb,Er@$mSiO_2$ group, no obvious difference was observed (Figure 4b bottom). Taken together, the ratiometric drug delivery system was successfully employed for drug release monitoring *in vitro*.

Internal Standard Effect of the Ratiometric Approach. The real-time local concentration of nanocarriers in biological samples is unknown and may even be dynamic, thus the internal standard within the ratiometric imaging based drug release monitoring approach has unique advantages compared to the single intensity approach. To illustrate these advantages, we conducted a comparative study by using two different concentrations of $NaYF_4$:Yb,Er@$mSiO_2$-DOX (0.1 mg/mL, 0.5 mg/mL) as shown in Figure 5. By comparing the single luminescence emission signal with UCL_G/UCL_R ratiometric images, we observed that the intensities of green and red upconversion emissions changed with the change of concentration of nanocarriers, while the intensities of ratiometric images were almost unaltered (Figure 5). Furthermore, the corresponding quantitative results are shown in the bar charts (right panel). The values of UCL_G/UCL_R were independent of

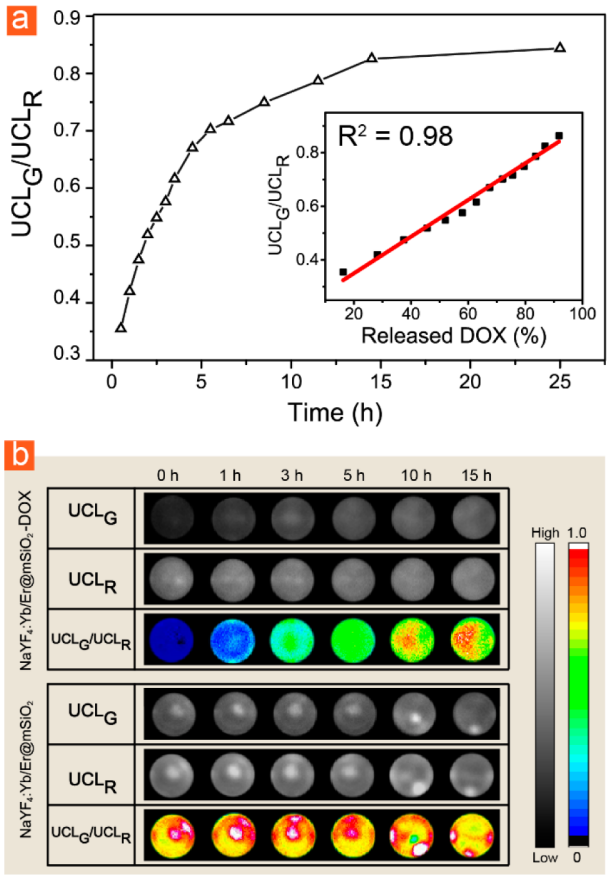

Figure 4. (a) UCL_G/UCL_R of $NaYF_4$:Yb,Er@$mSiO_2$-DOX as a function of time during the DOX release. Inset: curve of linear fitting UCL_G/UCL_R versus percent of cumulative released DOX. (b) UCL_G (500−600 nm), UCL_R (647−673 nm), and UCL_G/UCL_R channel images of $NaYF_4$:Yb,Er@$mSiO_2$-DOX and $NaYF_4$:Yb,Er@$mSiO_2$ in a 96-well plate as a function of time. The bar charts quantitatively represent the relative intensities of corresponding images either single luminescence emission or ratiometric imaging.

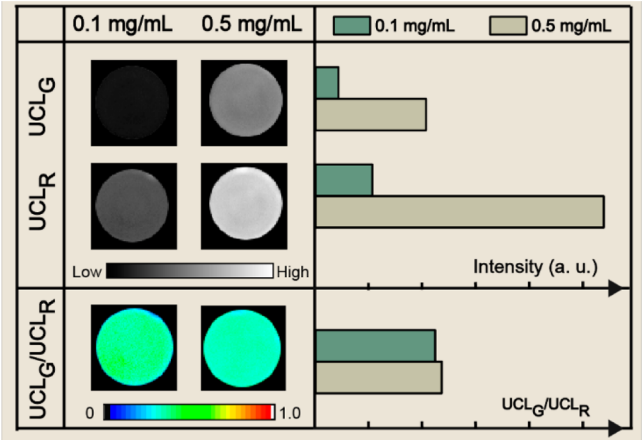

Figure 5. UCL_G (500−600 nm), UCL_R (647−673 nm), and UCL_G/UCL_R ratio images in a 96-well plate with different concentrations of $NaYF_4$:Yb,Er@$mSiO_2$-DOX (top panel) and $NaYF_4$:Yb,Er@$mSiO_2$ (bottom panel). The bar charts quantitatively represent the relative intensities of corresponding images of either single luminescence emission or ratiometric imaging.

the nanocarrier concentrations. Therefore, the ratiometric method could offer a practical and reliable platform for

DOI: 10.1021/acsami.5b03204
ACS Appl. Mater. Interfaces 2015, 7, 12278−12286

precisely monitoring the drug release kinetics in biological samples.

Evaluation of Cytotoxicity. In an attempt to assess the cytotoxicity of $NaYF_4$:Yb,Er@$mSiO_2$ nanoparticles, methyl thiazolyl tetrazolium (MTT) assay was conducted in HeLa cells involving different nanocarrier concentrations ranging from 12.5 to 400 g/mL. As shown in Figure 6, in the concentration ranges used in this study, no significant cytotoxicity was observed after the cells were incubated with $NaYF_4$:Yb,Er@$mSiO_2$ for 24 h, indicating the nanocarrier $NaYF_4$:Yb,Er@$mSiO_2$ has no obvious cytotoxicity. Therefore, it confirmed the proposal that the nanocarrier act merely as vehicles for the drug. Thus, any cytotoxicity observed mainly attributed to the effects of the released drug alone. In a parallel experiment, $NaYF_4$:Yb,Er@$mSiO_2$-DOX treated cells exhibited a dose-dependent cytotoxicity. When 200 μg/mL $NaYF_4$:Yb,Er@$mSiO_2$-DOX was incubated with the cells for 24 h, about 50% of cells died. This is mainly due to, following 24 h incubation, DOX released from the surface layer of the $NaYF_4$:Yb,Er@$mSiO_2$-DOX and led to cell death, which indicating the successful delivery of DOX into the cells.

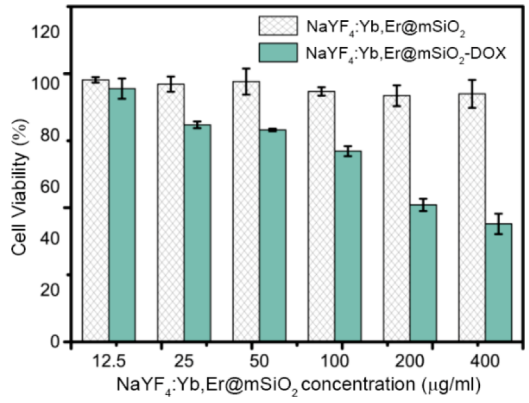

Figure 6. Cellular cytotoxicity studies by the MTT proliferation test versus different incubation concentration of $NaYF_4$:Yb,Er@$mSiO_2$ and $NaYF_4$:Yb,Er@$mSiO_2$-DOX.

Monitoring Intracellular Drug Release via Ratiometric Upconversion Imaging. To shed light on drug release monitoring in living cells, we recorded a set of laser scanning upconversion luminescence microscopy (LSUCLM)[44] images to visualize the intracellular drug release at 1, 3, 5, or 7 h (Figure 7). During the imaging process, the laser exposure time is shorter than 100 μs to avoid heat effect-induced cell damage. As presented in the second and third columns of Figure 7, a similar trend in the enhancement on UCL_G (510−560 nm) and UCL_R (630−690 nm) signals were observed as increasing in incubation time. It should be noted that the concentration of intracellular nanocarriers changed continually during the incubation period (the third column in Figure 7), as indicated by red upconversion luminescence, which was significant dependent on the $NaYF_4$:Yb,Er@$mSiO_2$ concentration. In this case, therefore, if a traditional single luminescent intensity-based method (For example, using UCL_G (510−560 nm) was chosen as signal), which may lead to unreliable or erroneous results for monitoring intracellular drug release, since intensity variation can be caused by the changing of intracellular nanocarriers amount.

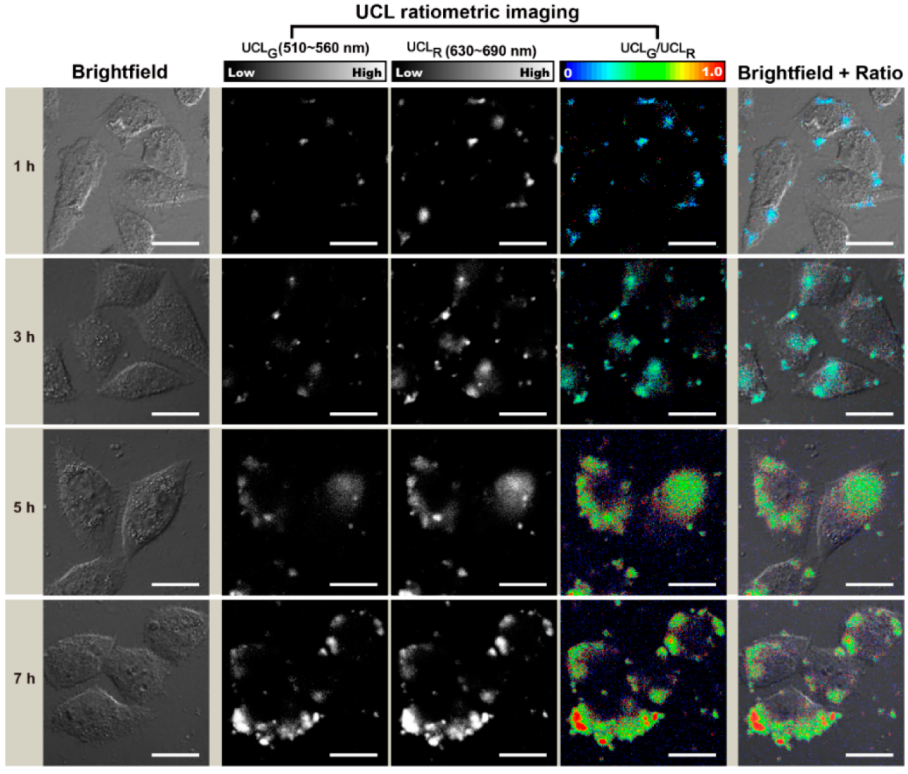

Figure 7. Confocal microscopic images of HeLa cells treated with $NaYF_4$:Yb,Er@mSiO2-DOX at selected emission channels in the course of DOX release time. Column 1, bright-field view; column 2, green upconversion emission signals; column 3, red upconversion emission signals; column 4, UCL_G/UCL_R ratiometric images; column 5, overlap of bright-field view and UCL_G/UCL_R ratiometric images. The scale bar: 20 μm.

DOI: 10.1021/acsami.5b03204
ACS Appl. Mater. Interfaces 2015, 7, 12278−12286

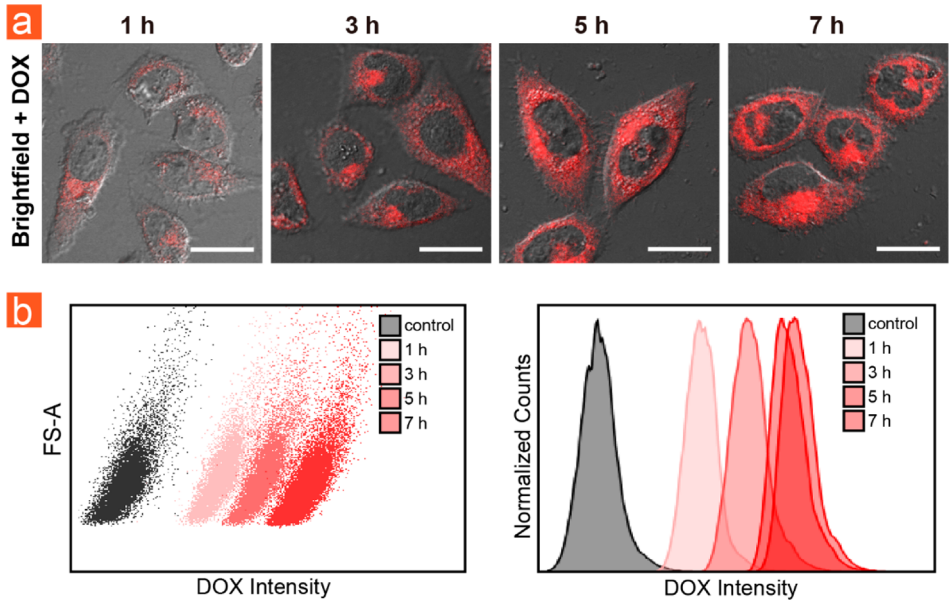

Figure 8. (a) Confocal fluorescence images of the cells incubated with $NaYF_4$:Yb,Er@$mSiO_2$-DOX at a different incubation time of 1, 3, 5, or 7 h. The fluorescence of DOX at 560−660 nm was collected under excitation at 488 nm. The scale bar: 20 μm. (b) Flow cytometry measurements for the intracellular accumulation of DOX released from $NaYF_4$:Yb,Er@$mSiO_2$-DOX (λ_{ex} = 488 nm, λ_{em} = 575 ± 25 nm).

By calculating the upconversion emission value of the 510−560 nm and 630−690 nm channels, UCL_G/UCL_R were visualized and expressed in the form of color images in the fourth column of Figure 7. A relatively low UCL_G/UCL_R value of 0.31 was observed after 1 h incubation of $NaYF_4$:Yb,Er@$mSiO_2$-DOX and then gradually increased over time. After 7 h, the UCL_G/UCL_R value (0.69) was close to the control group incubated with $NaYF_4$:Yb,Er@$mSiO_2$ (Figure S11 in the Supporting Information), indicating that DOX was almost completely released from the $NaYF_4$:Yb,Er@$mSiO_2$-DOX nanocarriers. Different from the single luminescent intensity-based method, the ratiometric UCL_G/UCL_R value only corresponds to the percentage of DOX released from the nanocarriers as indicated by the above-mentioned results. Therefore, our ratiometric method could offer more precise results during drug release monitoring by avoiding the local concentration effect of nanocarriers.

To examine the above monitoring results, we observed the signals of intracellular DOX fluorescence intensity (λ_{em} = 560−660 nm, under 488 nm excitation) using confocal fluorescent microscopy. During the course of incubation, DOX was released into the cytoplasm and entered into the cell nuclei, accompanied by an increase in fluorescence intensity (Figure 8a). In comparison, the control experiments showed faster accumulation of DOX in cells (Figure S12 in the Supporting Information). These results were also consistent with the intracellular DOX accumulation results quantified by flow cytometry. As shown in Figure 8b and Figure S13 in the Supporting Information, intracellular DOX accumulated in a delayed manner in $NaYF_4$:Yb,Er@$mSiO_2$-DOX treated group, whereas free DOX entered cells faster.

To further demonstrate the capabilities of our strategy, a semiquantitative analysis was also carried out by quantifying the pictorial information (Figure 9 and Figure S14 in the Supporting Information). The ratios of UCL_G/UCL_R were determined and plotted in Figure 9 (dotted line). Simultaneously, the fluorescent intensity value of DOX in the cells were also extracted (Figure 9, histogram). The results indicated

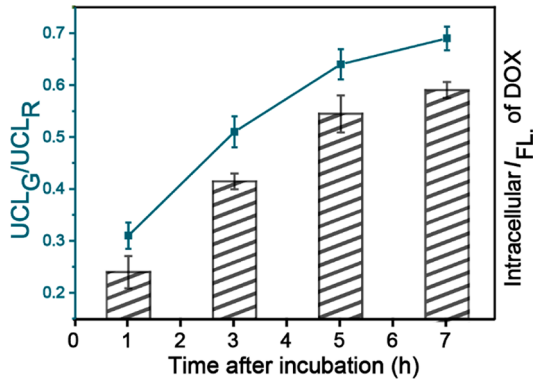

Figure 9. Corresponding semiquantitative results of UCL_G/UCL_R and intracellular fluorescence intensity (I_{FL}) of released DOX for cell images shown in Figure 7 column 4 and Figure 8a, respectively.

a consistent upward tendency during the process of DOX release. Taken together, these results suggest that our ratiometric design could be successfully employed for drug release monitoring in living cells with the avoidance of unknown local concentration effects.

CONCLUSION

In conclusion, a ratiometric upconversion approach was developed for monitoring drug release in living cells through upconversion-based luminescence resonance energy transfer (LRET) process. For DOX-loaded upconversion nanocomposite $NaYF_4$:Yb,Er@$mSiO_2$-DOX, a linear relationship between the UCL_G/UCL_R value and the amount of drug released was found and could be used as a standard curve to evaluate the drug-released efficiency. Complementary to conventional LRET-based drug release monitoring systems, our results enable a better understanding of drug release kinetics in living cells by excluding the unknown local concentration effect using red emission as the internal standard. The method can also be rationalized to visualize the process of drug delivery and extend

DOI: 10.1021/acsami.5b03204
ACS Appl. Mater. Interfaces 2015, 7, 12278−12286

for semiquantitative analysis in living cells. Therefore, the design offers new possibilities for advanced drug delivery research and clinical translation by expanding the pharmacy scope using abundant lanthanide-based luminescent nanomaterials with less cellular damage and deeper light penetration.

METHODS

Materials. The chemical of 1-octadecene (ODE, >90%), oleic acid (OA, >90%), and (3-aminopropyl) triethoxysilane (APS, 98%) were purchased from Alfa Aesar. Ammonium fluoride (NH_4F, 99.99%), sodium hydroxide (NaOH, 99.9%), acetic acid (95%), and tetraethylorthosilicate (TEOS, 99%) were obtained from Sinopharm. Hexadecyltrimethylammonium bromide (CTAB, 98%) was purchased from Aladdin Chemical Company, Inc. Rare-earth oxides (Ln_2O_3, 99.999%, $Ln^{3+} = Y^{3+}$, Er^{3+}, Yb^{3+}) were purchased from Beijing Lansu Co. Ltd. Doxorubicin (DOX) was purchased from Shanghai Hualan Chemical Company. All the chemicals were used as received unless otherwise noted. Deionized water was used throughout. Rare-earth chloride ($LnCl_3$, $Ln^{3+} = Y^{3+}$, Er^{3+}, Yb^{3+}) solutions were prepared at a concentration of 0.5 M by dissolving the corresponding Ln_2O_3 in hydrochloric acid at 120 °C.

Characterization. The morphology and size of the $NaYF_4$:Yb,Er and $NaYF_4$:Yb,Er@$mSiO_2$ particles were observed using a transmission electron microscope (TEM) (JEOL JEM-2010F, Japan). X-ray powder diffraction (XRD) measurements were carried out on a Bruker D4 diffractometer at a scanning rate of 1° min^{-1} in the 2θ range of 10−80°. Upconversion luminescence spectra was recorded on an Edinburgh LFS-920 spectrometer, where an 0−3 W tunable CW laser at 980 nm (Connet Fiber Optics, China) as the excitation source. Dynamic light scattering (DLS) experiments were performed on Zetasizer Nano (Malvern Instruments, Herrenberg, Germany).

Synthesis of Oleic Acid (OA) Coated $NaYF_4$:Yb,Er Nanoparticles (OA-$NaYF_4$:Yb,Er). OA-$NaYF_4$:Yb,Er nanoparticle was synthesized using the solvothermal procedure according to the previous report.[25] Typically, a solution of YCl_3 (0.78 mmol), $YbCl_3$ (0.20 mmol), $ErCl_3$ (0.02 mmol) was added into 8 mL of oleic acid and 15 mL of 1-octadecene mixture in a 100 mL flask. The resulting mixture was heated at 150 °C to form a homogeneous solution and then cooled down to room temperature. Shortly thereafter, 8 mL of methanol solution containing NaOH (2.5 mmol) and NH_4F (4 mmol) was slowly dropped into the flask and stirred for 45 min. Subsequently, the solution was slowly heated to 120 °C for 30 min to remove the methanol. The reaction was then heated to 300 °C under nitrogen protection and maintained for 1 h. The OA-$NaYF_4$:Yb,Er nanoparticle was collected by centrifugation at 8000 rpm for 15 min and washed with ethanol/cyclohexane three times prior to use.

Synthesis of Mesoporous Silica Coated $NaYF_4$:Yb,Er Nanocomposites ($NaYF_4$:Yb,Er@$mSiO_2$). $NaYF_4$:Yb,Er@$mSiO_2$ was synthesized via a modified procedure as described in detail in a previous report.[42] OA-$NaYF_4$:Yb,Er in cyclohexane was added in a CTAB aqueous solution (0.1 g, 20 mL of distilled water) and then stirred overnight at 30 °C. After the cyclohexane was evaporated, 10 mL of this $NaYF_4$:Yb,Er-CTAB solution was added to a round-bottom flask containing 20 mL of distilled water, 3 mL of ethanol, and 150 μL of NaOH solution (2 M). Thereafter, 200 μL of tetraethylorthosilicate (TEOS) was added to the above mixture and kept at 70 °C for 2 h before cooling down to room temperature. The resulting nanoparticles was washed with ethanol and centrifuged at 10 000 rpm 5 times. Subsequently, the obtained $NaYF_4$:Yb,Er@$mSiO_2$ nanoparticle was dispersed in 50 mL of ethanol solution containing 0.3 g of NH_4NO_3, stirred for 2 h to remove CTAB, and redispersed in ethanol.

DOX Loading. DOX loaded $NaYF_4$:Yb,Er@$mSiO_2$ nanoparticles ($NaYF_4$:Yb,Er@$mSiO_2$-DOX) were prepared as follows: briefly, 10 mg of $NaYF_4$:Yb,Er@$mSiO_2$ and 20 mg of DOX were dispersed in 5 mL of DMSO, followed by stirring at room temperature for 48 h, the resulting nanoparticles were precipitated by centrifugation at 14 000 rpm for 20 min and then dried in a vacuum oven for 24 h to remove DMSO. The as-prepared nanoparticles were then washed thoroughly with ethanol/water (1:19, v/v) until the supernatant was colorless and centrifuged at 8000 rpm for 15 min to obtained $NaYF_4$:Yb,Er@$mSiO_2$-DOX nanoparticles. An infrared spectrometer was used to monitor the loading of DOX in $NaYF_4$:Yb,Er@$mSiO_2$ nanoparticles.

***In Vitro* DOX Release.** In total, 2 mg of $NaYF_4$:Yb,Er@$mSiO_2$-DOX was dispersed in 4 mL of 0.9% NaCl and sealed in a boiled water pretreated dialysis bag (molecular weight cutoff (MWCO): 14 000). The dialysis bag was incubated with 18 mL of aqueous solution containing 0.9% NaCl and 0.5% tween 80 (w/w) in a 40 mL light-sealed tube. The tube was kept at 37 °C with gentle shaking at 200 rpm. To satisfy the sink condition, 2 mL of the incubation medium was extracted and an equal amount of fresh incubation medium was supplemented at certain time intervals. The concentration of released DOX was calculated using its absorption at 488 nm according to a standard curve.

***In Vitro* Monitoring of DOX Release.** Visualization of the *in vitro* drug release process was conducted using a small-animal UCL imaging system.[24] Specifically, the $NaYF_4$:Yb,Er@$mSiO_2$-DOX and $NaYF_4$:Yb,Er@$mSiO_2$ nanoparticles were added to a 96-well plate at predetermined time points during the drug release process. The imaging channels of green and red upconversion emission were 500−600 nm and 647−673 nm, respectively, upon excitation with a 980 nm laser. To illustrate the internal standard effect in the ratiometric approach, we studied single luminescence intensity and the UCL_G/UCL_R ratiometric images of nanocarriers ($NaYF_4$:Yb,Er@$mSiO_2$-DOX and $NaYF_4$:Yb,Er@$mSiO_2$) at different concentrations (0.1 mg/mL, 0.5 mg/mL). ImageJ was employed to calculate ratiometric images and quantitative measurements.

Cell Culture. Human epithelial cervical cancer cell line (HeLa) was provided by Shanghai Institutes for Biological Sciences (SIBS), Chinese Academy of Sciences (CAS, China). Cells were cultured in Dulbecco's modified Eagle's medium (DMEM) containing 10% fetal bovine serum (FBS), 100 units/mL penicillin G sodium, and 100 μg/mL streptomycin sulfate and maintained at 37 °C in a humidified and 5% CO_2 incubator.

Cell Viability Assays. The *in vitro* cytotoxicity of $NaYF_4$:Yb,Er@$mSiO_2$ and $NaYF_4$:Yb,Er@$mSiO_2$-DOX against HeLa cells were evaluated via the methyl thiazolyl tetrazolium (MTT) assay. Cells were seeded in 96-well cell-culture plate with a density of 1×10^4 per well and allowed to incubate for 12 h. After the medium was aspirated, the cells were treated with $NaYF_4$:Yb,Er@$mSiO_2$ and $NaYF_4$:Yb,Er@$mSiO_2$-DOX at various concentrations of 12.5, 25, 50, 100, 200, 400 μg/mL (100 μL/well) for the cytotoxicity study. Followed by incubation for 24 h, 20 μL of MTT (5 mg/mL) was added to each well and incubated for another 5 h. Then the medium was discarded and 100 μL of DMSO was added to each well to dissolve the formazan crystals. The absorption value of each well was measured at 570 nm by a Tecan Infinite M200, with a background subtraction at 690 nm. The viability of cell growth was determined by comparing the absorption value of the $NaYF_4$:Yb,Er@$mSiO_2$-DOX treated group with control wells.

Intracellular DOX Release and Confocal Microscopic Imaging. Confocal microscopy luminescence imaging was carried out using a modified OLYMPUS FV1000 laser scanning confocal fluorescence microscope. HeLa cells (1×10^4/dish) were seeded onto a glass coverslips in a 35 mm diameter culture dish and incubated for 12 h prior to experimentation. Thereafter, $NaYF_4$:Yb,Er@$mSiO_2$ and $NaYF_4$:Yb,Er@$mSiO_2$-DOX (200 μg/mL) were added to the culture dishes, respectively. Subsequently, confocal microscopy luminescence imaging was taken at scheduled times. DOX fluorescence was detected at 530−630 nm under excitation at 488 nm. Upconversion luminescence of $NaYF_4$:Yb,Er nanoparticles was detected at 500−600 nm for green emission (UCL_G) and at 600−700 nm for red emission (UCL_R), under excitation at 980 nm. ImageJ was employed for image calculation and quantitative measurements.

Flow Cytometry Analysis. Here, a flow cytometer was utilized to quantitatively determine the intracellular accumulation of DOX. HeLa cells were exposed to free DOX and $NaYF_4$:Yb,Er@$mSiO_2$-DOX for 1, 3, 5, and 7 h, respectively. The treated cells were then washed thoroughly and stored in PBS buffer prior to analysis. The flow cytometer (Gallios, Beckman Coulter) was conducted with excitation

DOI: 10.1021/acsami.5b03204
ACS Appl. Mater. Interfaces 2015, 7, 12278−12286

and detection wavelength set at λ_{ex} = 488 nm and λ_{em} = 575 ± 25 nm, respectively, and the obtained results were analyzed by FlowJo.

■ ASSOCIATED CONTENT

Supporting Information

XRD pattern, DLS, EDX, elemental mapping analysis, FTIR spectra of nanoparticles, drug-loading related information, and results of control groups. The Supporting Information is available free of charge on the ACS Publications website at DOI: 10.1021/acsami.5b03204.

■ AUTHOR INFORMATION

Corresponding Author

*E-mail: fyli@fudan.edu.cn. Fax: +86 21 55663270.

Author Contributions

The manuscript was written through contributions of all authors. All authors have given approval to the final version of the manuscript.

Funding

The authors acknowledge the financial support from MOST of China (Grant Nos. 2015CB931800 and 2012CB932403), National Science Foundation of China (Grant Nos. 21231004 and 91027004), Shanghai Sci. Tech. Comm. (Grant Nos. 12JC1401300, 13NM1401101, and 10431903100), and The CAS/SAFEA International Partnership Program for Creative Research Teams.

Notes

The authors declare no competing financial interest.

■ REFERENCES

(1) Kim, C. S.; Tonga, G. Y.; Solfiell, D.; Rotello, V. M. Inorganic Nanosystems for Therapeutic Delivery: Status And Prospects. *Adv. Drug Delivery Rev.* **2013**, *65*, 93−99.

(2) Bao, G.; Mitragotri, S.; Tong, S. Multifunctional Nanoparticles for Drug Delivery and Molecular Imaging. *Annu. Rev. Biomed. Eng.* **2013**, *15*, 253−282.

(3) De Koker, S.; Hoogenboom, R.; De Geest, B. G. Polymeric Multilayer Capsules for Drug Delivery. *Chem. Soc. Rev.* **2012**, *41*, 2867−2884.

(4) Doane, T. L.; Burda, C. The Unique Role of Nanoparticles in Nanomedicine: Imaging, Drug Delivery and Therapy. *Chem. Soc. Rev.* **2012**, *41*, 2885−2911.

(5) Pancholi, K. A Review of Imaging Methods for Measuring Drug Release at Nanometre Scale: A Case for Drug Delivery Systems. *Expert Opin. Drug Delivery* **2012**, *9*, 203−218.

(6) Drummond, D. C.; Noble, C. O.; Hayes, M. E.; Park, J. W.; Kirpotin, D. B. Pharmacokinetics and *in vivo* Drug Release Rates in Liposomal Nanocarrier Development. *Eur. J. Pharm. Sci.* **2008**, *97*, 4696−4740.

(7) Brannon-Peppas, L.; Blanchette, J. O. Nanoparticle and Targeted Systems for Cancer Therapy. *Adv. Drug Delivery Rev.* **2012**, *64*, 206−212.

(8) Lai, J.; Shah, B. P.; Garfunkel, E.; Lee, K.-B. Versatile Fluorescence Resonance Energy Transfer-Based Mesoporous Silica Nanoparticles for Real-Time Monitoring of Drug Release. *ACS Nano* **2013**, *7*, 2741−2750.

(9) Gui, R.; Wan, A.; Zhang, Y.; Li, H.; Zhao, T. Ratiometric and Time-Resolved Fluorimetry from Quantum Dots Featuring Drug Carriers for Real-Time Monitoring of Drug Release *in situ*. *Anal. Chem.* **2014**, *86*, 5211−5214.

(10) Chen, K. J.; Chiu, Y. L.; Chen, Y. M.; Ho, Y. C.; Sung, H. W. Intracellularly Monitoring/Imaging the Release of Doxorubicin from Ph-Responsive Nanoparticles Using Forster Resonance Energy Transfer. *Biomaterials* **2011**, *32*, 2586−2592.

(11) Weinstain, R.; Segal, E.; Satchi-Fainaro, R.; Shabat, D. Real-time Monitoring of Drug Release. *Chem. Commun. (Cambridge, U. K.)* **2010**, *46*, 553−555.

(12) Jana, A.; Devi, K. S.; Maiti, T. K.; Singh, N. D. Perylene-3-Ylmethanol: Fluorescent Organic Nanoparticles as a Single-Component Photoresponsive Nanocarrier with Real-Time Monitoring of Anticancer Drug Release. *J. Am. Chem. Soc.* **2012**, *134*, 7656−7659.

(13) Lee, M. H.; Kim, J. Y.; Han, J. H.; Bhuniya, S.; Sessler, J. L.; Kang, C.; Kim, J. S. Direct Fluorescence Monitoring of the Delivery and Cellular Uptake of a Cancer-Targeted Rgd Peptide-Appended Naphthalimide Theragnostic Prodrug. *J. Am. Chem. Soc.* **2012**, *134*, 12668−12674.

(14) Laine, A. L.; Gravier, J.; Henry, M.; Sancey, L.; Bejaud, J.; Pancani, E.; Wiber, M.; Texier, I.; Coll, J. L.; Benoit, J. P.; Passirani, C. Conventional versus Stealth Lipid Nanoparticles: Formulation and *in Vivo* Fate Prediction through Fret Monitoring. *J. Controlled Release* **2014**, *188*, 1−8.

(15) Cui, W.; Lu, X.; Cui, K.; Wu, J.; Wei, Y.; Lu, Q. Fluorescent Nanoparticles of Chitosan Complex for Real-Time Monitoring Drug Release. *Langmuir* **2011**, *27*, 8384−8390.

(16) Chen, H.; Kim, S.; Li, L.; Wang, S.; Park, K.; Cheng, J. X. Release of Hydrophobic Molecules from Polymer Micelles into Cell Membranes Revealed by Forster Resonance Energy Transfer Imaging. *Proc. Natl. Acad. Sci. U.S.A.* **2008**, *105*, 6596−6601.

(17) Gulin-Sarfraz, T.; Sarfraz, J.; Didem Şen, K.; Zhang, J.; Oetken-Lindholm, C.; Duchanoy, A.; Rosenholm, J. M.; Abankwa, D. FRET-reporter Nanoparticles to Monitor Redox-induced Intracellular Delivery of Active Compounds. *R. Soc. Chem. Adv.* **2014**, *4*, 16429−16437.

(18) Chen, W.; Huang, Q.; Ou, W.; Hao, Y.; Wang, L.; Zeng, K.; Guo, H.; Li, J.; Liu, Y.-N. Self-Reporting Liposomes for Intracellular Drug Release. *Small* **2014**, *10*, 1261−1265.

(19) Feng, W.; Han, C.; Li, F. Upconversion-nanophosphor-based functional nanocomposites. *Adv. Mater.* **2013**, *25*, 5287−5303.

(20) Zhou, J.; Liu, Z.; Li, F. Upconversion Nanophosphors for Small-animal Imaging. *Chem. Soc. Rev.* **2012**, *41*, 1323−1349.

(21) Chen, G.; Qiu, H.; Prasad, P. N.; Chen, X. Upconversion Nanoparticles: Design, Nanochemistry, and Applications in Theranostics. *Chem. Rev.* **2014**, *114*, 5161−5214.

(22) Yang, Y.; Zhao, Q.; Feng, W.; Li, F. Luminescent Chemodosimeters for Bioimaging. *Chem. Rev.* **2013**, *113*, 192−270.

(23) Liu, Q.; Feng, W.; Li, F. Water-soluble Lanthanide Upconversion Nanophosphors: Synthesis and Bioimaging Applications *in Vivo*. *Coord. Chem. Rev.* **2014**, *273*−*274*, 100−110.

(24) Liu, Q.; Feng, W.; Yang, T.; Yi, T.; Li, F. Upconversion Luminescence Imaging of Cells and Small Animals. *Nat. Protoc.* **2013**, *8*, 2033−2044.

(25) Zhao, L.; Peng, J.; Huang, Q.; Li, C.; Chen, M.; Sun, Y.; Lin, Q.; Zhu, L.; Li, F. Near-Infrared Photoregulated Drug Release in Living Tumor Tissue via Yolk-Shell Upconversion Nanocages. *Adv. Funct. Mater.* **2014**, *24*, 363−371.

(26) Fan, Y.; Li, C.; Cao, H.; Li, F.; Chen, D. The Intranuclear Release of a Potential Anticancer Drug from Small Nanoparticles that are Derived from Intracellular Dissociation of Large Nanoparticles. *Biomaterials* **2012**, *33*, 4220−4228.

(27) Yang, D.; Kang, X.; Ma, P. A.; Dai, Y.; Hou, Z.; Cheng, Z.; Li, C.; Lin, J. Hollow Structured Upconversion Luminescent $NaYF_4$: Yb^{3+}, Er^{3+} Nanospheres for Cell Imaging and Targeted Anti-Cancer Drug Delivery. *Biomaterials* **2013**, *34*, 1601−1612.

(28) Wang, C.; Cheng, L.; Liu, Y.; Wang, X.; Ma, X.; Deng, Z.; Li, Y.; Liu, Z. Imaging-Guided pH-sensitive Photodynamic Therapy Using Charge Reversible Upconversion Nanoparticles under Near-Infrared Light. *Adv. Funct. Mater.* **2013**, *23*, 3077−3086.

(29) Hou, Z.; Li, C.; Ma, P. a.; Cheng, Z.; Li, X.; Zhang, X.; Dai, Y.; Yang, D.; Lian, H.; Lin, J. Up-Conversion Luminescent and Porous $NaYF_4$:Yb^{3+},Er^{3+}@$mSiO_2$ Nanocomposite Fibers for Anti-Cancer Drug Delivery and Cell Imaging. *Adv. Funct. Mater.* **2012**, *22*, 2713−2722.

DOI: 10.1021/acsami.5b03204
ACS Appl. Mater. Interfaces 2015, 7, 12278−12286

(30) Fan, N.-C.; Cheng, F.-Y.; Ho, J.-a.; Yeh, C.-S. Photocontrolled Targeted Drug Delivery: Photocaged Biologically Active Folic Acid as a Light-responsive Tumor-targeting Molecule. *Angew. Chem., Int. Ed.* **2012**, *51*, 8806−8810.
(31) Xu, H.; Cheng, L.; Wang, C.; Ma, X.; Li, Y.; Liu, Z. Polymer Encapsulated Upconversion Nanoparticle/iron Oxide Nanocomposites for Multimodal Imaging and Magnetic Targeted Drug Delivery. *Biomaterials* **2011**, *32*, 9364−9373.
(32) Kang, X.; Cheng, Z.; Li, C.; Yang, D.; Shang, M.; Ma, P. a.; Li, G.; Liu, N.; Lin, J. Core−Shell Structured Up-Conversion Luminescent and Mesoporous $NaYF_4$:Yb^{3+}/Er^{3+}@nSiO_2@mSiO_2 Nanospheres as Carriers for Drug Delivery. *J. Phys. Chem. C* **2011**, *115*, 15801−15811.
(33) Xiong, L.; Chen, Z.; Tian, Q.; Cao, T.; Xu, C.; Li, F. High Contrast Upconversion Luminescence Targeted Imaging *in vivo* Using Peptide-Labeled Nanophosphors. *Anal. Chem.* **2009**, *81*, 8687−8694.
(34) Sun, Y.; Peng, J.; Feng, W.; Li, F. Upconversion Nanophosphors NaLuF(4):Yb,Tm For Lymphatic Imaging *in Vivo* by Real-Time Upconversion Luminescence Imaging under Ambient Light and High-Resolution X-ray CT. *Theranostics* **2013**, *3*, 346−353.
(35) Peng, J.; Sun, Y.; Zhao, L.; Wu, Y.; Feng, W.; Gao, Y.; Li, F. Polyphosphoric Acid Capping Radioactive/upconverting $NaLuF_4$:Yb,Tm,^{153}Sm Nanoparticles for Blood Pool Imaging *in Vivo*. *Biomaterials* **2013**, *34*, 9535−9544.
(36) Liu, Y.; Chen, M.; Cao, T.; Sun, Y.; Li, C.; Liu, Q.; Yang, T.; Yao, L.; Feng, W.; Li, F. A Cyanine-modified Nanosystem for *in Vivo* Upconversion Luminescence Bioimaging of Methylmercury. *J. Am. Chem. Soc.* **2013**, *135*, 9869−9876.
(37) Liu, J.; Bu, J.; Bu, W.; Zhang, S.; Pan, L.; Fan, W.; Chen, F.; Zhou, L.; Peng, W.; Zhao, K.; Du, J.; Shi, J. Real-time *in Vivo* Quantitative Monitoring of Drug Release by Dual-mode Magnetic Resonance and Upconverted Luminescence Imaging. *Angew. Chem., Int. Ed.* **2014**, *53*, 4551−4555.
(38) Hou, Z.; Li, X.; Li, C.; Dai, Y.; Ma, P.; Zhang, X.; Kang, X.; Cheng, Z.; Lin, J. Electrospun Upconversion Composite Fibers as Dual Drugs Delivery System with Individual Release Properties. *Langmuir* **2013**, *29*, 9473−9482.
(39) Dai, Y.; Yang, D.; Ma, P.; Kang, X.; Zhang, X.; Li, C.; Hou, Z.; Cheng, Z.; Lin, J. Doxorubicin Conjugated NaYF(4):Yb(3+)/Tm(3+) Nanoparticles for Therapy and Sensing of Drug Delivery by Luminescence Resonance Energy Transfer. *Biomaterials* **2012**, *33*, 8704−8713.
(40) Guo, H.; Idris, N. M.; Zhang, Y. LRET-based Biodetection of DNA Release in Live Cells Using Surface-modified Upconverting Fluorescent Nanoparticles. *Langmuir* **2011**, *27*, 2854−2860.
(41) Jiang, S.; Zhang, Y. Upconversion Nanoparticle-based FRET System for Study of siRNA in Live Cells. *Langmuir* **2010**, *26*, 6689−6694.
(42) Li, C.; Liu, J.; Alonso, S.; Li, F.; Zhang, Y. Upconversion Nanoparticles for Sensitive and In-depth Detection of Cu^{2+} Ions. *Nanoscale* **2012**, *4*, 6065−6071.
(43) Ray, P. C.; Fan, Z.; Crouch, R. A.; Sinha, S. S.; Pramanik, A. Nanoscopic Optical Rulers Beyond the FRET Distance Limit: Fundamentals and Applications. *Chem. Soc. Rev.* **2014**, *43*, 6370−6404.
(44) Yu, M.; Li, F.; Chen, Z.; Hu, H.; Zhan, C.; Yang, H.; Huang, C. Laser Scanning Up-conversion Luminescence Microscopy for Imaging Cells Labeled with Rare-earth Nanophosphors. *Anal. Chem.* **2009**, *81*, 930−935.

DOI: 10.1021/acsami.5b03204
ACS Appl. Mater. Interfaces 2015, 7, 12278−12286